Proceedings of IMECE2005
2005 ASME International Mechanical Engineering Congress and Exposition
November 5-11, 2005, Orlando, Florida USA

IMECE2005-80962

ANALYTICAL AND EXPERIMENTAL STUDIES OF ORTHOTROPIC CORNER-SUPPORTED PLATES WITH SEGMENTED IN-PLANE ACTUATORS

Hartono Sumali, Jordan E. Massad, Phillip L. Reu, Pavel M. Chaplya, and Jeffrey W. Martin
Sandia National Laboratories
Albuquerque, NM 87185-1310
hsumali@sandia.gov

ABSTRACT

This paper outlines a model for a corner-supported, thin, rectangular bimorph actuated by a two-dimensional array of segmented, orthotropic PVDF laminates; it investigates the realization and measurement of such a bimorph. First, a model is derived to determine the deflected shape of an orthotropic laminate for a given distribution of voltages over the actuator array. Then, boundary conditions are realized in a laboratory setup to approach the theoretical corner-supported boundary condition. Finally, deflection measurements of actuated orthotropic PVDF laminates are performed with Electronic Speckle Pattern Interferometry and are compared to the model results.

NOMENCLATURE

$\mathbf{A}$	Energy expansion diagonal matrix with k^{th} diagonal component A_k, [N/m]
$\mathbf{A}^{act}$	Actuation expansion matrix, [N/V]
$\mathbf{a}$	Vector of first expansion coefficients with k^{th} component a_k, [m]
a	Length of bimorph in x direction, [m]
$\mathbf{B}$	Energy expansion diagonal matrix with k^{th} diagonal component B_k, [N/m]
$\mathbf{B}^{act}$	Actuation expansion matrix, [N/V]
$\mathbf{b}$	Vector of second expansion coefficients with k^{th} component b_k, [m]
b	Length of bimorph in y direction, [m]
$\mathbf{C}$	Energy expansion matrix with jk^{th} component C_{jk}, [N/m]
c_p	Coefficient of p^{th} Zernike polynomial, [m]
d_{31}, d_{32}	Piezoelectric strain constants, [m/V]
D_{11}, D_{12}, D_{22}, D_{66}	Plate stiffness constants, [N·m]
D_e	Bonding layer stiffness constant, [N·m]
D_s	Electrode layer stiffness constant, [N·m]
D_{act}	Actuator stiffness constant, [N·m/V]
G_{12}	Orthotropic shear modulus of actuator layers, [Pa]
h	Shortest distance between electrodes, [m]
h_e	Thickness of epoxy bonding layer, [m]
h_p	Thickness of actuator layer, [m]
h_s	Thickness of electrode layer, [m]
i_{max}	Number of actuator segments
k	Mode number
k_{max}	Number of modes included in calculation
m_k	number of half sinusoids of mode k in the x direction
n_k	number of half sinusoids of mode k in the y direction
N	Number of Zernike fit data points
$\mathbf{V}$	Vector of voltages with i^{th} component V_i, [V]
$w(x,y)$	Deflection, [m]
x	Lengthwise coordinate, [m]
x_{1_i}, x_{2_i}	x position of right, left of segment i, [m]
Y_{11}, Y_{22}	Orthotropic Young's moduli of actuator layers, [Pa]
Y_e	Young's modulus of bonding layer, [Pa]
Y_s	Young's modulus of electrode layer, [Pa]
y	Widthwise coordinate, [m]
y_{1_i}, y_{2_i}	y positions of bottom, top of segment i, [m]
Z_p	p^{th} Zernike polynomial
z	Through-thickness coordinate, [m]
γ_j , χ_{jk}	Orthogonality parameters

ν_{12}, ν_{21}	Orthotropic Poisson ratios of actuator layers
ν_e	Poisson ratio of bonding layer
ν_s	Poisson ratio of electrode layers

INTRODUCTION

Thin, flexible piezoelectric bimorphs can be used as optical reflectors and radio antennae. The need for very large space-based aperture reflectors in small lightweight packages has given rise to a concept where a bimorph sheet mirror is rolled before launch, deployed in orbit, and then adaptively actuated into the desired shape using a computed distribution of electric field. In this design, rectangular sheets offer an area advantage over circular sheets. With rectangular reflectors, the corner-supported boundary condition offers certain advantages over the edge-supported boundary conditions. Corner-supported adaptive structures allow for natural actuation into parabolic geometries, greater flexibility, and larger achievable deflections when compared to the more commonly studied edge-supported geometries. Moreover, with a simple uniform distributed electric field, corner supports results in actuation into a paraboloid, which is the most important geometry for reflectors.

Polyvinylidene fluoride (PVDF) has been identified as a flexible piezoelectric material suitable for reflector shape control (Jenkins, 2000; Washington, 1996). The process of polarizing piezoelectric PVDF involves stretching extruded thin polymer sheets, thereby aligning molecular chains in the stretch direction. PVDF film has orthotropic electromechanical properties mainly because of unidirectional stretching in the fabrication (Vinogradov, 2002). In shape control applications where PVDF is the actuated surface and a symmetric material response is preferred, the orthotropic nature of PVDF needs to be considered.

This paper outlines a model for a corner-supported, thin, rectangular bimorph actuated by a two-dimensional array of segmented, orthotropic PVDF laminates and it investigates the realization and measurement of such a bimorph. In Section 2, a model is derived to determine the deflected shape of an orthotropic laminate for a given distribution of voltages over the actuator array. In Section 3, boundary conditions are established for a fabricated PVDF laminate in a laboratory setup and deflection measurements are performed with Electronic Speckle Pattern Interferometry (ESPI). The experimental results are compared to the model results. Finally, in Section 4, parabolic deflection of the actuated bimorph is demonstrated with a Zernike polynomial analysis.

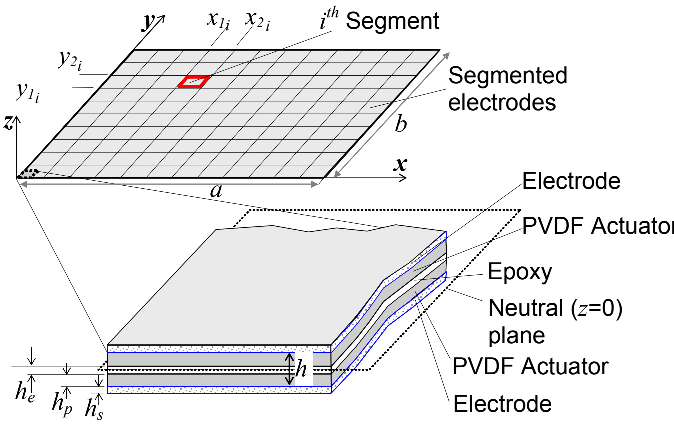

Figure 1: PVDF Bimorph with Segmented Electrodes

2. A METHOD FOR CALCULATING THE DEFLECTION OF AN ORTHOTROPIC LAMINATE

Figure 1 is a sketch of the flexible mirror, which is modeled as five layers. The top and bottom layers are metal electrodes. The thickness of these layers is h_s. The second and fourth layers are piezoelectric PVDF of thickness h_p. The middle layer is a bonding layer made of material such as epoxy of thickness h_e. The electrodes are segmented as shown in the figure. Each segment will be actuated with a certain electric field. The three-layer laminate is fabricated such that the polarization of the top piezoelectric layer is the opposite of the polarization of the bottom piezoelectric layer. Furthermore, the bottom PVDF layer is oriented 90° with respect to the top PVDF layer so that the polymer stretching direction for the bottom layer is along the y-axis. As shown in Massad *et al.* (2005), the 90° orientation of the orthotropic material allows the laminate to actuate collectively as an isotropic material.

Electric voltage V_i is applied on the top surface of the top layer, and the bottom of the bottom layer is grounded. On segment i, this voltage results in an electric field $E_i = V_i/h$, where h is the shortest distance between the electrodes. The electric field E_i does not change signs throughout the whole thickness of the laminate. When the top layer expands as a result of E_i, the bottom layer contracts, thereby creating bimorph bending. This section summarizes a method derived in Massad *et al.* (2005) to calculate the deflection of the laminate for a given distribution of segment voltages.

We write the deflection $w(x,y)$ of a corner-supported plate as (Reed *et al.*, 1965; Sumali *et al.*, 2004)

$$w(x,y) = \sum_{j=1}^{k_{\max}} \phi_j(x,y), \tag{1}$$

where

$$\phi_j(x,y) = a_j \cos\left(m_j \pi \frac{x}{a}\right) \sin\left(n_j \pi \frac{y}{b}\right) + \\ + b_j \cos\left(m_j \pi \frac{y}{b}\right) \sin\left(n_j \pi \frac{x}{a}\right). \quad (2)$$

The indices m_j and n_j are non-negative- and positive integers, respectively. The coefficients a_j and b_j resulting from a given distribution of segment voltages can be obtained using the following technique.

First, compute plate stiffness constants

$$D_{11} = D_e + D_s + \\ + \frac{(Y_{11} + Y_{22}) h_p}{12(1 - \nu_{12}\nu_{21})}\left(4h_p^2 + 6h_p h_e + 3h_e^2\right), \quad (3)$$

$$D_{12} = \nu_e D_e + \nu_s D_s + \\ + \frac{\nu_{12} Y_{22} h_p}{6(1 - \nu_{12}\nu_{21})}\left(4h_p^2 + 6h_p h_e + 3h_e^2\right), \quad (4)$$

$$D_{66} = \frac{1-\nu_e}{2} D_e + \frac{1-\nu_s}{2} D_s + \\ + \frac{G_{12} h_p}{6}\left(4h_p^2 + 6h_p h_e + 3h_e^2\right), \quad (5)$$

and $D_{22} = D_{11}$. The contributions from the bonding- and electrode layers are

$$D_e = \frac{Y_e h_e^3}{12(1 - \nu_e^2)} \quad (6)$$

and

$$D_s = \frac{Y_s h_s}{6(1 - \nu_s^2)}\left(3h^2 + 6hh_s + 4h_s^2\right), \quad (7)$$

respectively. Additionally, compute the actuator stiffness constant

$$D_{act} = \frac{Y_{22} h_p (h_p + h_e)}{2(1 - \nu_{12}\nu_{21})}\left[\left(\frac{Y_{11}}{Y_{22}} + \nu_{12}\right) d_{31} + (1 + \nu_{12}) d_{32}\right]. \quad (8)$$

Then, compute the following constants for each index j:

$$A_j = \frac{\pi^4}{4a^3b^3}\left[D_{11} b^4 m_j^{\,4} + 2(D_{12} + 2D_{66}) a^2 b^2 m_j^{\,2} n_j^{\,2} + \\ + \gamma_j D_{22} a^4 n_j^{\,4}\right] \quad (9)$$

$$B_j = \frac{\pi^4}{4a^3b^3}\left[\gamma_j D_{11} b^4 n_j^{\,4} + 2(D_{12} + 2D_{66}) a^2 b^2 m_j^{\,2} n_j^{\,2} + \\ + D_{22} a^4 m_j^{\,4}\right]. \quad (10)$$

In addition, where $m_j \neq n_k$ and $m_k \neq n_j$,

$$C_{jk} = \frac{2\pi^2}{a^3b^3} \frac{\chi_{jk} n_j n_k}{(m_j^{\,2} - n_k^{\,2})(m_k^{\,2} - n_j^{\,2})} \times \\ \times \left[D_{11} b^4 m_j^{\,2} n_k^{\,2} + (D_{12} + 4D_{66}) a^2 b^2 m_j^{\,2} m_k^{\,2} + \\ D_{12} a^2 b^2 n_j^{\,2} n_k^{\,2} + D_{22} a^4 m_k^{\,2} n_j^{\,2}\right]. \quad (11)$$

Otherwise, $C_{jk} = 0$. The orthogonality parameters are

$$\gamma_j = \begin{cases} 2 & m_j = 0 \\ 1 & otherwise \end{cases} \quad (12)$$

and

$$\chi_{jk} = \left[(-1)^{m_j + n_k} - 1\right]\left[(-1)^{n_j + m_k} - 1\right]. \quad (13)$$

Finally, the actuation constants are calculated over the i-th actuator region $\in (x_{1_i}, x_{2_i}) \times (y_{1_i}, y_{2_i})$ depicted in Figure 1.

$$A_j^{act_i} = \begin{cases} 4\left(\frac{an_j}{bm_j} + \frac{bm_j}{an_j}\right) \sin\left(m_j \pi \frac{x_{2_i} - x_{1_i}}{2a}\right) \cos\left(m_j \pi \frac{x_{2_i} + x_{1_i}}{2a}\right) \times \\ \times \sin\left(n_j \pi \frac{y_{2_i} - y_{1_i}}{2b}\right) \sin\left(n_j \pi \frac{y_{2_i} + y_{1_i}}{2b}\right) & m_j \neq 0 \\ 2\pi n_j \frac{(x_{2_i} - x_{1_i})}{b} \sin\left(n_j \pi \frac{y_{2_i} - y_{1_i}}{2b}\right) \sin\left(n_j \pi \frac{y_{2_i} + y_{1_i}}{2b}\right) & m_j = 0 \end{cases} \quad (14)$$

and

$$B_j^{act_i} = \begin{cases} 4\left(\frac{am_j}{bn_j} + \frac{bn_j}{am_j}\right) \sin\left(n_j \pi \frac{x_2 - x_1}{2a}\right) \sin\left(n_j \pi \frac{x_2 + x_1}{2a}\right) \times \\ \times \sin\left(m_j \pi \frac{y_2 - y_1}{2b}\right) \cos\left(m_j \pi \frac{y_2 + y_1}{2b}\right) & m_j \neq 0 \\ 2\pi n_j \frac{(y_2 - y_1)}{a} \sin\left(n_j \pi \frac{x_2 - x_1}{2a}\right) \sin\left(n_j \pi \frac{x_2 + x_1}{2a}\right) & m_j = 0. \end{cases} \quad (15)$$

Next, form the matrix $\mathbf{C} \in \Re^{j_{max} \times j_{max}}$ containing C_{jk}, and the diagonal matrices $\mathbf{A}, \mathbf{B} \in \Re^{j_{max} \times j_{max}}$ containing A_j and B_j, respectively. Also form $\mathbf{A}^{act}, \mathbf{B}^{act} \in \Re^{j_{max} \times i_{max}}$ containing $\frac{D_{act}}{h} A_j^{act_i}$ and $\frac{D_{act}}{h} B_j^{act_i}$, respectively, and form the vector of given voltages $\mathbf{V} \in \Re^{i_{max}}$. Finally, solve the linear system

$$\begin{bmatrix} \mathbf{C} & \mathbf{2B} \\ \mathbf{2A} & \mathbf{C} \end{bmatrix} \begin{bmatrix} \mathbf{a} \\ \mathbf{b} \end{bmatrix} = \begin{bmatrix} \mathbf{B}^{\mathbf{act}} \\ \mathbf{A}^{\mathbf{act}} \end{bmatrix} \mathbf{V} \quad (16)$$

for the unknowns $\mathbf{a}, \mathbf{b} \in \Re^{j_{max}}$ containing the coefficients a_j and b_j. Once these coefficients are obtained, Eqs. (1) and (2) give the deflection of the bimorph.

The method outlined in this section was applied to a bimorph with properties listed in Table 1. The predicted deflection is shown in the left part of Figure 2. In the experiment described in Section 3, a single-segmented bimorph was used to implement a voltage distribution that was uniform throughout the bimorph. As shown in Massad *et al.*(2004), a uniform actuation voltage distribution results in paraboloid shape. The paraboloid is the most important shape for the intended optical reflector application.

Table 1: Bimorph parameters.

Layer	Actuator	Bonding	Electrode
Material	PVDF	Epoxy	Silver ink
Thickness [μm]	h_p=52	h_e=120	h_s=18
Modulus [GPa]	Y_{11}=2.70	Y_e =1.20	Y_s =0.81
	Y_{22}=2.50		
	G_{12}=0.935		
Poisson Ratio	ν_{12}=0.326	ν_e=0.350	ν_s=0.350
	ν_{21}=0.302		
Piezoelectric constants [pm/V]	d_{31}=23		
	d_{32}=2.3		
x Length [mm]	83		
y Length [mm]	83		
No. of segments in x			1
No. of segments in y			1

3. EXPERIMENTAL INVESTIGATION

3.1 Experimental Setup

The bimorph described in Table 1 was fabricated and then attached to a frame between two plates of glass as shown on the right side of Figure 3. The corners of the bimorph were fabricated with small tabs that were fixed to the frame. The deflection was measured using ESPI with an out-of-plane measurement resolution better than 45 nm. This high sensitivity causes two experimental complications: vibration sensitivity and limited total deformation measurement per voltage step (i.e., only a limited number of fringes may be measured per step). The fixture addresses the vibration concerns by providing protection from parasitic vibrations and acoustic noise that hinder the fringe measurement. A total actuation voltage of 300 V was applied through the electrodes in approximately 5 V steps to limit the number of fringes obtained per step.

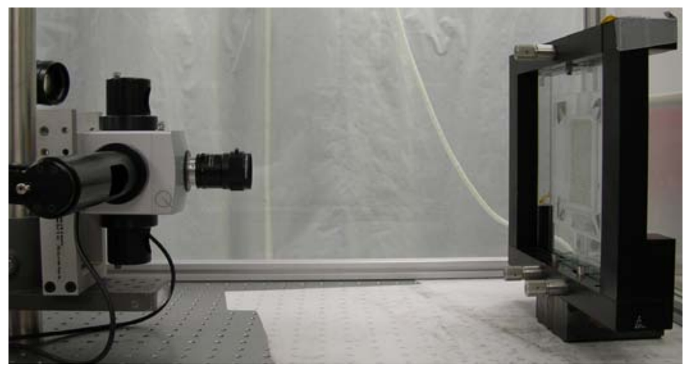

Figure 3: ESPI system and bimorph experimental setup.

3.2 Measured Deflections

The ESPI results from each step were summed to yield the total distortion plot. The results for 300 V actuation are shown Figure 2. Qualitatively, the measured deflection appears to be similar to the predicted analytical deflection. The most

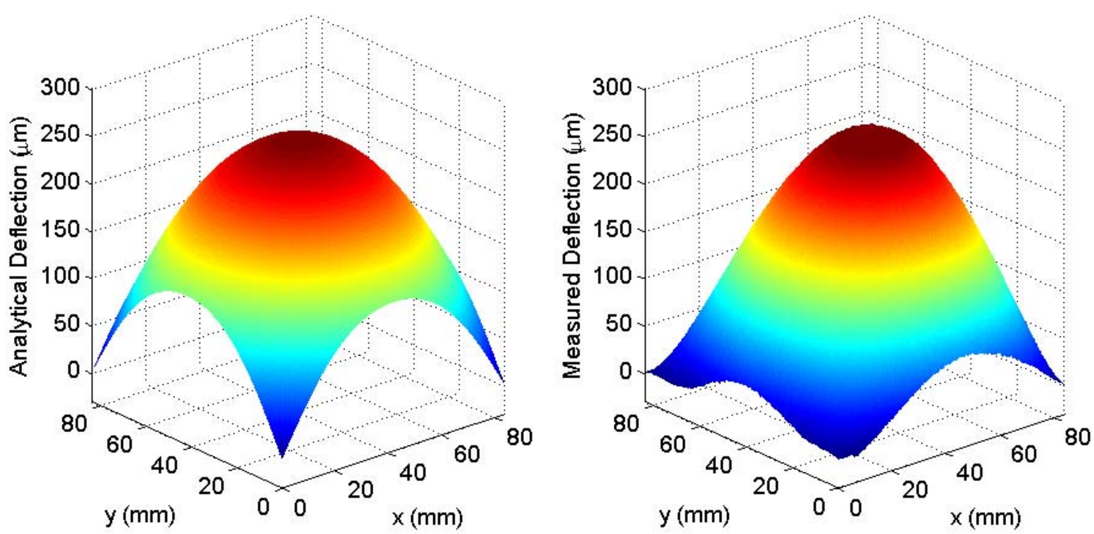

Figure 2: Bimorph out-of-plane deformation from simulation (left) and experimental results (right).

significant differences are in the edge deflections. The finite size and stiffness of the tabs and pinned condition of the tabs is a likely source of the reduced deflection of the fabricated bimorph. In addition, it was observed that edge deflections are highly sensitive to pretension in the bimorph due to fixturing. Also, measurement showed that the thickness at numerous points on the bimorph was not uniform. The following section quantifies the similarity between the measured deflection and the intended paraboloid shape.

4. PARABOLOID NATURE OF THE DEFLECTION

4.1 Zernike Polynomial Fit

Previous work has shown numerically that uniform actuation results in paraboloid shape (Massad *et al.*, 2004). A convenient way to examine the paraboloid nature of an optical reflector is to express deflection in the Zernike basis. In the case of the deflection in the experiment, the measured deflection w^{meas} is expressed as a weighted sum of orthogonal Zernike polynomial basis functions Z_p

$$w^{meas}(x,y) \approx w^{fit}(r,\varphi) = \sum_{p=1}^{p_{\max}} c_p Z_p(r,\varphi). \tag{17}$$

The Zernike expansion is in a polar coordinate system, which is related to the rectangular coordinate system of the measured data as follows.

$$r = \sqrt{x_{norm}^2 + y_{norm}^2} \tag{18}$$

and

$$\varphi = \tan^{-1}\left(\frac{y_{norm}}{x_{norm}}\right), \tag{19}$$

where

$$x_{norm} = \frac{x-(a/2)}{a/2} \tag{20}$$

and

$$y_{norm} = \frac{y-(b/2)}{b/2}. \tag{21}$$

Figures 4-5 give the definitions and illustrations of the 12 lowest-order Zernike basis functions Z_p (p = 1, ..., 12). Other Zernike functions used here can be deduced from the ones shown in the figures. For example, the tetrafoil 0° function is the tetrafoil 45° function rotated 45°. In this analysis, the domain of the Zernike basis functions is limited to the circle $(r \in [0,1], \varphi \in [0,2\pi])$. Recall that the rectangular bimorph spans the physical domain $(x \in [0,a], y \in [0,b])$. Therefore, the corners of the bimorph are not included in the Zernike series expansion of the deflection. The corners of the bimorph are used for mechanical support and will not be used in the optics. Another reason for limiting the fit to the circular domain will be shown below after the discussion on the fitting procedure.

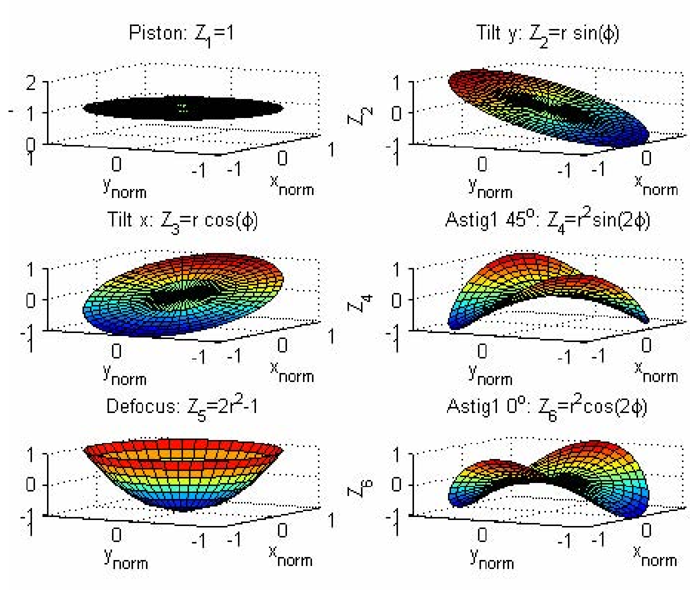

Figure 4: Definitions and illustrations of Zernike basis functions 1-6 used in expressing the measured deflections.

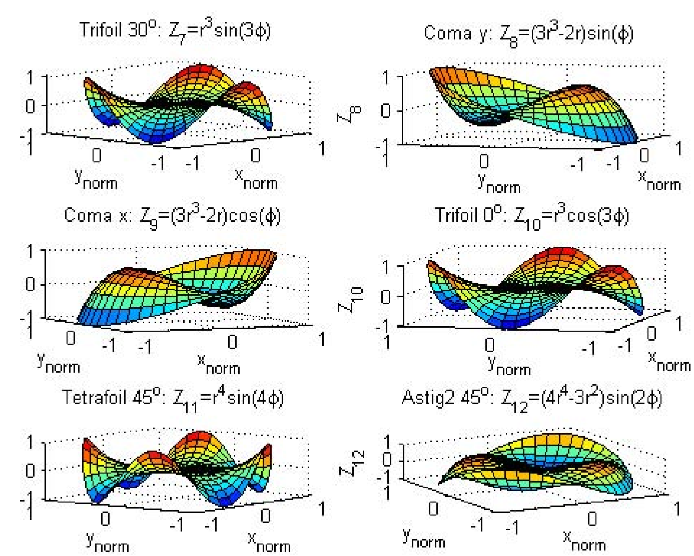

Figure 5: Definitions and illustrations of Zernike basis functions 7-12 used in expressing the measured deflections.

The Zernike coefficients c_p in Eq. (17) are obtained via least squares. First, a cost function is expressed as

$$J_{Zern} = \sum_{n=1}^{N}\left(w_n^{fit} - w_n^{meas}\right)^2, \tag{22}$$

where w_n^{fit} is the Zernike expansion deflection from Eq. (17) evaluated at the n-th discretization point of the domain, w_n^{meas} is the corresponding measured deflection, and N is the total number of discretization points. Minimizing J_{Zern} with respect to the expansion coefficients c_p results in a system of p_{max} linear equations

$$\left(\sum_{n=1}^{N}\begin{bmatrix} Z_1(r_n,\varphi_n)^2 & Z_1(r_n,\varphi_n)Z_2(r_n,\varphi_n) & \cdots & Z_1(r_n,\varphi_n)Z_{p_{\max}}(r_n,\varphi_n) \\ Z_1(r_n,\varphi_n)Z_2(r_n,\varphi_n) & Z_2(r_n,\varphi_n)^2 & & \\ \vdots & & \ddots & \\ Z_1(r_n,\varphi_n)Z_{p_{\max}}(r_n,\varphi_n) & & & Z_1(r_n,\varphi_n)Z_{p_{\max}}(r_n,\varphi_n) \end{bmatrix}\right)\begin{bmatrix} c_1 \\ c_2 \\ \vdots \\ c_{p_{\max}} \end{bmatrix} = \sum_{n=1}^{N}\begin{bmatrix} w(x_n,y_n)Z_1(r_n,\varphi_n) \\ w(x_n,y_n)Z_2(r_n,\varphi_n) \\ \vdots \\ w(x_n,y_n)Z_{p_{\max}}(r_n,\varphi_n) \end{bmatrix} \quad (23)$$

that can be solved for c_p. The matrix in the above equation will be diagonal provided that the fit data is limited to the circular sub-domain $(r \in [0,1], \varphi \in [0,2\pi])$ of the bimorph, because the Zernike polynomials are orthogonal in the unit circle. For future analytical studies, this orthogonality offers some advantage of limiting the fit to the circular sub-domain.

Figure 6 shows the Zernike expansion coefficients c_p for the measured deflection as functions of the applied voltage. The piston, tilt-x and tilt-y components have been removed from the data. It is clear that the deflections consist mainly of the "defocus" Z_5 term in Figure 4, which is the paraboloid component. The largest distortion from the paraboloid shape comes from the tetrafoil 0^o term, which means that the largest errors are around the corners. This suggests that the four corner supports are not perfect.

4.2 Focal Length as a Function of Actuation Voltage

One of the most important characteristics of optical reflectors is the focal length. For a circular parabola of diameter a, the focal length can be shown to be related to the coefficient c_5 of the defocus Zernike by

$$L_f = \frac{a^2}{32c_5}. \quad (24)$$

Thus, for the bimorph tested here the actuation voltage controlled the focal length from $L_f = \infty$ for $V = 0$ to $L_f = 2.34$ m for $V = 300$ V.

6. CONCLUSION

In this paper, a method was outlined and used to compute the deflection of a bimorph reflector actuated with a uniformly distributed voltage. The deflection caused by a uniform voltage profile was predicted to be of a paraboloid shape. A bimorph was fabricated, mounted, and tested with ESPI. The predicted deflection agreed qualitatively with the measured deflection. Other shapes can be realized and will be analyzed and tested in future investigations, however improvements in bimorph fabrication and boundary condition realization must be sought.

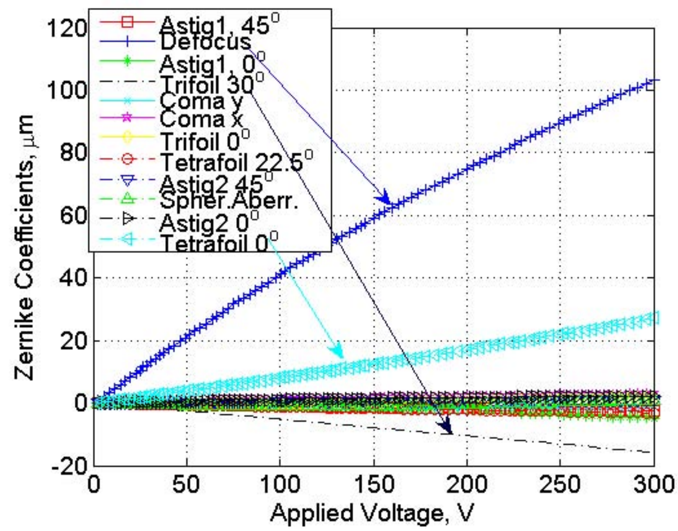

Figure 6: Measured deflections in terms of Zernike polynomial coefficients.

7. ACKNOWLEDGMENTS

The authors are grateful for the technical assistance of Gregory Washington. This work was conducted at Sandia National Laboratories. Sandia is a multi-program laboratory operated under Sandia Corporation, a Lockheed Martin Company, for the United States Department of Energy under Contract DE-AC04-94-AL85000.

8. REFERENCES

C.H. Jenkins and A.M. Vinogradov, 2000, "Active polymers for space applications," *IEEE Aerospace Conference Proceedings*, pp. 415-420.

J.E. Massad, G.N. Washington and H. Sumali , 2005, "Orthotropic deflection model for corner-supported plates with segmented in-plane actuators," *Proc. SPIE*, 5757, pp. 503-514.

J.E. Massad, H. Sumali, J. W. Martin, and P.M. Chaplya, 2004, "Deflection model for corner-supported plates with segmented in-plane actuators," *Proc. SPIE*, 5383, pp. 309-319.

R.E. Reed, "Comparison of methods in calculating frequencies of corner-supported rectangular plates," NASA Technical Report, NASA-TN-D-3030, 1965.

H. Sumali, J.E. Massad, J. W. Martin, and P.M. Chaplya, 2004, "Deflection Control of a Corner-supported Plate Using Segmented In-plane Actuators," *Proc. ASME IMECE* 2004-61141.

A. Vinogradov, 2002, "Piezoelectricity in Polymers," in M. Schwartz (Ed.), *Encyclopedia of Smart Materials*, pp. 781-792, J. Wiley, New York.

G. Washington, 1996, "Smart aperture antennas," *Smart Materials and Structures*, **5**(6), pp. 801-805.

